J. Fluid Mech. (1991), *vol.* 226, *pp.* 37–61
Printed in Great Britain

Moving loads on ice plates of finite thickness

By J. STRATHDEE†, W. H. ROBINSON AND E. M. HAINES
Physics and Engineering Laboratory, DSIR, Lower Hutt, New Zealand

(Received 21 November 1988 and in revised form 31 May 1990)

The response of a floating ice plate to a moving load is given in terms of a pair of Green's functions. General expressions for these Green's functions are derived for the case of an infinite isotropic plate of uniform thickness supported on a fluid base of uniform depth. The distributions of stress and strain in the vicinity of a concentrated load receive significant contributions from waves of length comparable with the plate thickness and their description necessitates an exact description of thickness effects. Circumstances in which the classical thin-plate theory can be recovered are discussed. The steady-state response to a uniformly moving load displays a so-called 'critical' behaviour for load velocities in the neighbourhood of a threshold value at which radiation commences. At the critical speed the amplitude is limited by dissipative forces in the ice plate. To describe this a simple viscoelastic term is included in our model. Calculations indicate that thin-plate theory is accurate to within 5% for distances greater than twenty times the ice thickness.

1. Introduction

To describe and predict the behaviour of a floating sheet of ice under the action of a moving load is a matter of some practical importance. In both the Arctic and Antarctic regions the sea ice is driven over by vehicles and used for runways by light aircraft and planes as heavy as 150 tonnes (C141 Starlifters). In the cold regions of the northern hemisphere, lake ice is driven over by logging trucks and leisure vehicles. Heavy, stationary structures such as sleeping quarters and drilling rigs have also been mounted on sea ice.

A number of experimental and theoretical investigations have appeared over the years. Early work is surveyed by Kerr (1976). See also Doronin & Kheisin (1977), Eyre (1977), Beltaos (1981), Davys, Hosking & Sneyd (1985), Squire *et al.* (1985), Takizawa (1985). Our purpose here is to describe some elaborations of the classical theoretical model (Nevel 1970). These elaborations, which are concerned with the effects of damping and finite plate thickness, are needed for the interpretation of some recently obtained data from Antarctica (Squire *et al.* 1988). These include measurements of the strain induced in a 2 m thick ice sheet at distances of 1 to 800 m from the path of vehicles moving at speeds of up to 90 km/h and low-flying aircraft (<300 km/h). Some of the measurements are from points relatively close to the path, and their theoretical representation cannot depend on the use of asymptotic approximations or the neglect of thickness effects. It is therefore necessary to go beyond the Euler–Bernoulli type of approximation and to treat the ice sheet as an elastic plate of finite thickness. Other measurements refer to vehicle speeds near to the so-called 'critical' value of ~ 70 km/h. This critical value corresponds to a

† On leave of absence from ICTP, Trieste, Italy.

threshold at which radiative phenomena set in. The classical model for the steady-state behaviour fails at the critical point owing to its neglect of dissipative effects. To describe the critical response it is essential to include such effects (Hosking, Sneyd & Waugh 1988). For these reasons we undertake a theoretical description here which includes both thickness and damping effects. We shall not treat the experimental data as they will be dealt with in a later paper.

There are many uncertainties in applying a simple model to describe the observed data. Among these are the effects of irregularities in the thickness and composition of the ice sheet, in its temperature distribution and mechanical properties. The underlying water will generally be layered (Schulkes, Hosking & Sneyd 1987). There may be currents and non-uniformities on the bottom, islands, edges, etc. There may be a significant amount of pre-stress (Kerr 1983) due to water and air currents. Some of the data may be contaminated by transient effects such as the acceleration of the load, which at this stage, we are not prepared to accommodate. In the case of static loads it will be important to consider plastic (creep) as well as elastic behaviour.

Many severe and probably unrealistic simplifications are made in the model discussed here. Although it has been shown that time-dependent effects may be important in interpreting experimental data (Schulkes & Sneyd 1988), we shall deal only with a uniformly moving load and its associated steady-state response pattern. The ice is modelled by an isotropic plate of uniform thickness supported on an incompressible, non-viscous fluid base of uniform depth and composition. On the upper surface of the plate a moving load is distributed. The resulting strain distribution is to be described.

The problem divides naturally into two parts. Firstly, there is the response of the elastic plate to the applied surface forces: the load on the upper face and the fluid stresses on the lower face. Secondly, there is the fluid motion governed by the boundary conditions on the bottom and at the surface where it supports the plate.

The elastic plate is taken to be isotropic but not necessarily thin. It is characterized by several parameters: two elastic moduli, mass density, thickness and frictional parameters. For most purposes it would be enough to restrict consideration to waves that are long in comparison with plate thickness. The plate motion is largely flexural and the classical Euler–Bernoulli description is adequate. One of our aims, however, is to describe the response of the plate to a concentrated load. If the load size is small enough, then waves of length comparable with the plate thickness will be significant, at least in the vicinity of the load itself. Such waves are not adequately described by the classical theory. For example, the maximum strain tends to grow logarithmically with inverse load size in the classical theory, but quadratically in the more exact theory. To show this we shall treat the plate as a three-dimensional isotropic material with prescribed distributions of force on its upper and lower faces. In the horizontal direction it extends to infinity. A very efficient method for treating this kind of problem has been developed for seismic waves (Kennett 1983) and we shall use it in §2.

The boundary forces on the lower face are due to the action of the fluid. To obtain them it is necesary to solve the fluid problem subject to the condition that the fluid joins smoothly to the lower surface of the plate. One then computes the fluid stress tensor at the interface. The end result of this computation is a set of equations relating boundary forces to plate displacements on the lower surface.

The water will be treated as an incompressible non-viscous fluid in the linear regime of the Navier–Stokes equation. It is characterized by two parameters: density and depth. For most purposes the viscosity can be neglected. However, viscosity is

easily allowed for and a treatment including it is given by Strathdee, Robinson & Haines (1989).

Previous treatments of this kind of system have generally been restricted by the thin-plate approximation. Waves of length comparable with or smaller than the plate thickness are neglected. There are two independent justifications for this. Firstly, the load distribution may be sufficiently 'soft', i.e. such that its Fourier representation is composed of long waves only. Alternatively, even when the load is concentrated, the response at sufficiently large distances can be dominated by long waves. There are two questions concerning the validity of the thin-plate approximation. First, in what circumstances is the response at sufficiently large distances dominated by long waves? We shall show that for the thin-plate approximation to be mathematically consistent it is necessary that a certain dimensionless coupling parameter should be small:

$$\beta^2 = (1-\nu)\frac{\rho g h}{G} \ll 1, \tag{1.1}$$

where ρ is the density of water, g the acceleration due to gravity, h is the plate thickness, G is the shear modulus, and ν is Poisson's ratio. For the Antarctic sea ice, parameter values of which are given in table 1, β^2 is of order 10^{-6} and we expect the thin-plate approximation to give an accurate description at sufficiently large distances. However, to describe the near-field strain pattern it will be necessary to retain the short-wave contributions and work with finite-thickness-plate theory. Second, what is a sufficiently long distance? Because of the complexity of the thick-plate expressions, this can only be answered by calculating the thick-plate solutions numerically and comparing them with the thin-plate solutions. Our calculations for stationary loads indicate that thin-plate theory is accurate to within 5% for distances greater than twenty times the ice thickness.

When the load is moving with constant velocity, and the transients have died away, the resulting steady-state response is best described in a co-moving frame of reference where it appears as a stationary wave pattern. The pattern clearly depends on the speed, U, of the load and its forward–backward asymmetry will increase with the speed. There is a critical speed, U_c, below which the wave amplitude falls exponentially with distance from the load. This decay law, $\exp(-r/l)$, defines a characteristic length, l, given approximately by

$$l = (6\beta^2)^{-\frac{1}{4}}h = \left(\frac{D}{\rho g}\right)^{\frac{1}{4}}, \tag{1.2}$$

where $D = Eh^3/12(1-\nu^2)$ is the flexural rigidity of the ice plate and E is its Young's modulus (Nevel 1970). For greater speeds, $U > U_c$, energy is radiated and the wave amplitude falls like $r^{-\frac{1}{2}}$. The dominant waves in the radiation have lengths of order l. Near the threshold speed, $U \sim U_c$, the response is limited by internal friction in the ice sheet (Squire & Allan 1980; Bates & Shapiro 1981). In the treatment to be described in the following, the internal friction is allowed for by using complex frequency-dependent elastic moduli. We find that the wave amplitude at critical speed is proportional to $\tau^{-\frac{1}{4}}$ and that it is exponentially damped on a distance scale $\propto \tau^{-\frac{1}{2}}$, where τ is a relaxation time. As the speed is increased the forward–backward asymmetry is accentuated. The waves represent coupled modes of the elastic plate and the fluid base: the forward component is progressively dominated by shorter elastic waves and the backward component by longer, gravity waves. At higher

$h = 2$ m	plate thickness
$H = 300$ m	sea depth
$\rho = 1040$ kg m^{-3}	water density
$m = 850$ kg m^{-3}	ice density
$G = 3 \times 10^9$ J m^{-3}	shear modulus
$D = 6 \times 10^9$ J	flexural rigidity
$\nu = 0.3$	Poisson's ratio
$\beta = 2 \times 10^{-3}$	coupling parameter
$l = 28$ m	characteristic length
$(gl)^{\frac{1}{2}} = 17$ ms^{-1}	characteristic speed
$(gH)^{\frac{1}{2}} = 55$ ms^{-1}	upper critical speed
$\tilde{q}(0) = 10^4$N–10^6N	total load
$(l/g)^{\frac{1}{2}} \sim 1$ s	characteristic time for motion
$u = 0$–100 m/s	vehicle speed

TABLE 1. Typical sea ice parameters

speeds the pattern develops caustics, a kind of bow wave. There is an upper threshold speed U_{c1}, at which the backward wave becomes infinitely long. For $U > U_{c1}$ the backward wave is extinguished. A 'shadow region' develops (Davys *et al.* 1985) in which the pattern is exponentially damped on the scale, $l((U^2/U_{c1}^2)-1)^{-\frac{1}{2}}$. The upper critical speed is given by $U_{c1} = (gH)^{\frac{1}{2}}$, where H is the fluid depth. (This threshold is contained in the range covered by the Antarctica data, Squire *et al.* 1988.)

The general theory is set out in §2 where the thick-plate problem is solved in terms of a pair of Green's functions. By this we mean that the distributions of stress and strain throughout the plate are represented by Fourier integrals involving Green's function kernels folded with a loading distribution. The stationary limit and, in particular, its asymptotic form is considered in §3. Here it is possible to see clearly how the exact solution deviates from the thin-plate approximation in the vicinity of the load. Section 4 is devoted to a more general consideration of the asymptotic distribution for the steadily moving load. The important consequences of damping in the ice for the threshold behaviour are discussed. In §5 we present some numerical examples. Some conclusions and discussion are given in §6.

2. Formulation

The dynamical variables of the system are two vectors, the plate displacement, u_α, and the fluid velocity, v_α. We suppose that the plate is uniform and isotropic, that the displacements are small enough for linear elastic theory to apply, and that there is no pre-stress. The fluid, of uniform depth and composition, in inviscid and incompressible.

The coordinate system is chosen so that, at equilibrium, the fluid surface and plate underface coincide with the plane, $z = 0$. The upper face of the plate is given by $z = h > 0$ and the bottom of the fluid by $z = -H < 0$. Fluid and plate extend without limit in the (x, y)-directions (see figure 1).

The components of the stress tensor, $T_{\alpha\beta}$, are constructed from the dynamical variables, u_α and v_α:

$$T_{\alpha\beta}^{\text{plate}} = G\left(\partial_\alpha u_\beta + \partial_\beta u_\alpha + \frac{2\nu}{1-2\nu}\delta_{\alpha\beta}\partial_\gamma u_\gamma\right), \quad 0 < z \leqslant h \tag{2.1a}$$

$$T_{\alpha\beta}^{\text{fluid}} = -p\delta_{\alpha\beta}, \qquad -H \leqslant z < 0 \tag{2.1b}$$

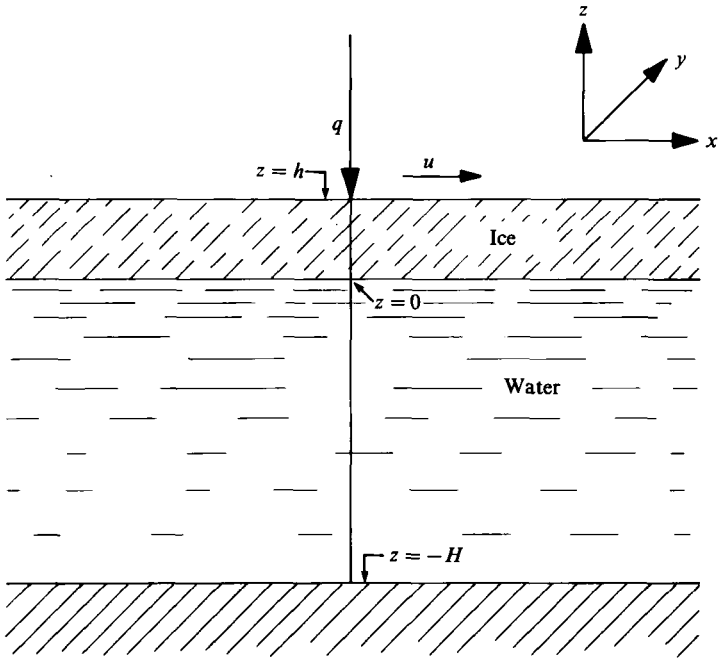

FIGURE 1. Diagram of floating ice sheet, showing a uniaxial load q moving with a velocity u in the x-direction.

where the shear modulus G and Poisson's ratio ν may be complex and frequency dependent.

In these expressions Greek indices α, β, γ refer to the coordinate axes, x, y, z. Partial derivatives are indicated by $\partial_\alpha = \partial/\partial x^\alpha$ and the summation convention is assumed, $\partial_\gamma u_\gamma = \partial_x u_x + \partial_y u_y + \partial_z u_z$. It will be useful in the following to distinguish the z-axis and use italic indices for the x, y axes, e.g. $\partial_j u_j = \partial_x u_x + \partial_y u_y$.

To complete the dynamics we need the mass densities, m for the plate and ρ for the fluid. The equations of motion are then given, in the linear regime, by

$$m\,\partial_t^2 u_\beta = \partial_\alpha T_{\alpha\beta} - \partial_\beta (mgz), \quad 0 < z \leqslant h, \tag{2.2a}$$

$$\rho\,\partial_t v_\beta = \partial_\alpha T_{\alpha\beta} - \partial_\beta (\rho g z), \quad -H \leqslant z < 0. \tag{2.2b}$$

By considering the equilibrium of a small volume which straddles the interface, $z = 0$, one obtains the condition that $T_{z\alpha}$ should be continuous there,

$$T_{z\alpha}^{\text{fluid}} = T_{z\alpha}^{\text{plate}}, \quad z = 0. \tag{2.3}$$

In addition it is assumed that there is no cavitation of the fluid relative to the plate,

$$v_z = \partial_t u_z, \quad z = 0. \tag{2.4}$$

At the bottom the normal fluid velocity is assumed to vanish,

$$v_z = 0, \quad z = -H. \tag{2.5}$$

The boundary data are completed by prescribing a load distribution on the upper face of the plate. For simplicity we shall assume a uniaxial stress in the vertical direction,

$$T_{zz} = q, \quad T_{zj} = 0, \quad z = h. \tag{2.6}$$

The aim of this calculation is to find expressions for the strain components,

$$S_{\alpha\beta} = \tfrac{1}{2}(\partial_\alpha u_\beta + \partial_\beta u_\alpha)$$

near the upper face. One needs to compute these components for various loads, q. In view of the symmetries of this problem, it is natural to use Fourier integral representations with respect to x, y and t,

$$q(x, y, t) = \int \frac{\mathrm{d}^2k\,\mathrm{d}\omega}{(2\pi)^3} \tilde{q}(k, \omega)\, \mathrm{e}^{\mathrm{i}(\omega t - k_j x_j)}. \tag{2.7}$$

The end result of the dynamical computation will then be integral expressions for the required components,

$$S_{\alpha\beta}|_{z=h} = \int \frac{\mathrm{d}^2k\,\mathrm{d}\omega}{(2\pi)^3} G_{\alpha\beta}(k, \omega)\, \tilde{q}(k, \omega)\, \mathrm{e}^{\mathrm{i}(\omega t - k_j x_j)}, \tag{2.8}$$

where Green's function, $G_{\alpha\beta}(k, \omega)$ incorporates the various parameters and boundary conditions introduced above. The exact form of $G_{\alpha\beta}$ is complicated and our interest is mainly in approximations. It is worth mentioning, however, that both $G_{\alpha\beta}$ and $\tilde{q}$ can be analytically continued in k_j and ω. They are both real analytic in the sense

$$\tilde{q}(k, \omega)^* = \tilde{q}(-k^*, -\omega^*), \tag{2.9}$$

and $G_{\alpha\beta}$ must be free of singularities in the region, $\operatorname{Im}\omega < 0, \operatorname{Im} k_j = 0$.

For the case of a uniformly moving load there is a simplification. Suppose the load is applied at $t = 0$ and thereafter moves with constant speed, U, in the x-direction,

$$q(x, y, t) = \begin{cases} 0 & , \quad t < 0, \\ q(x - Ut, y), & t > 0. \end{cases} \tag{2.10}$$

The Fourier transform of this loading is given by the inverse of (2.7),

$$\begin{aligned} \tilde{q}(k, \omega) &= \int_0^\infty \mathrm{d}t \int_{-\infty}^\infty \mathrm{d}^2x q(x - Ut, Y)\, \mathrm{e}^{\mathrm{i}(k_j x_j - \omega t)} \\ &= \left[\pi\delta(\omega - Uk_x) + \frac{\mathrm{i}}{\omega - Uk_x}\right] \tilde{q}(k), \end{aligned} \tag{2.11}$$

where $\tilde{q}(k)$ is the two-dimensional Fourier transform of $q(x, y)$. On substituting (2.11) into (2.8) and integrating over ω, various terms arise. Those associated with singularities of $G_{\alpha\beta}$ are transients and will eventually die away. Only the singularity of $q(k, \omega)$ at $\omega = Uk_x$, will persist as t becomes large. It will give rise to the steady-state pattern,

$$S_{\alpha\beta} = \int \frac{\mathrm{d}^2k}{(2\pi)^2} G_{\alpha\beta}(k, Uk_x)\, \tilde{q}(k)\, \mathrm{e}^{-\mathrm{i}(k_x(x - Ut) - \mathrm{i}k_y y)}. \tag{2.12}$$

In a coordinate system co-moving with the load, the dependence on t disappears.

The computation of $G_{\alpha\beta}(k, \omega)$ involves a rather lengthy analysis of the system (2.1)–(2.6). In the following we shall treat the equivalent problem of computing the components of the displacement vector u_α and stress tensor $T_{\alpha\beta}$. We shall deal firstly with the fluid, the purpose being to compute $T_{z\alpha}$ at $z = 0$ in terms of the velocities, $\partial_t u_\alpha$. This information is then used as input for the plate problem.

The velocity and pressure distributions in the incompressible fluid are obtained by solving the equation of motion (2.2*b*) or

$$\rho\,\partial_t v_\beta = -\partial_\beta(p+\rho g z)$$

together with the continuity condition

$$\partial_\beta v_\beta = 0$$

subject to the boundary conditions (2.4) and (2.5). By introducing a velocity potential ϕ such that $\boldsymbol{v} = \nabla\phi$, it is straightforward to solve this system for wave-like modes. The calculation is essentially the same as that for gravity waves in water of uniform depth (see, for example, Lighthill 1978). This solution for irrotational flow has a non-zero tangential velocity at the boundaries. In a viscous fluid all components of the fluid velocity are zero at a solid boundary; however, the non-viscous solution can still apply in a viscous fluid if there is a thin dissipative boundary layer between the irrotational flow and the surface (Lighthill 1978). When the results are substituted into (2.1*b*) at $z = 0$ one obtains, using the boundary condition (2.4),

$$\tilde{T}_{zz} = \left(\rho g - \frac{\rho\omega^2}{k\,\mathrm{th}\,(kH)}\right)\tilde{u}_z, \tag{2.13a}$$

$$\tilde{T}_{zj} = 0, \tag{2.13b}$$

where $k = (k_x^2+k_y^2)^{\frac{1}{2}}$ and th denotes the hyperbolic tangent.

These equations are now to be thought of as boundary conditions on the plate stress at $z = 0$.

For the plate dynamics it is useful to follow the method of the seismologists (Kennett 1983) and arrange the equations of motion in the form of first-order differential equations in z (after Fourier transforming with respect to x, y and t). In this arrangement the displacements, u_α, and stress components, $T_{z\alpha}$, are treated as independent variables. In effect, the equations (2.1*a*) and (2.2*a*) are on the same footing. For $0 \leqslant z \leqslant h$, eliminating the subsidiary variables T_{ij} using the ∂_z-independent equations contained in (2.1*a*), one writes

$$\left.\begin{aligned}
\partial_z u_z &= \frac{1}{2G}\frac{1-2\nu}{1-\nu}T_{zz} - \frac{\nu}{1-\nu}\partial_j u_j,\\
\partial_z u_j &= \frac{1}{G}T_{zj} - \partial_j u_z,\\
\partial_z T_{zz} &= -\partial_j T_{zj} - m\omega^2 u_z,\\
\partial_z T_{zj} &= -\frac{\nu}{1-\nu}\partial_j T_{zz} - G\left(-\omega^2 u_j + \frac{1+\nu}{1-\nu}\partial_j\partial_k u_k\right) + m\,\partial_t^2 u_j,
\end{aligned}\right\} \tag{2.14}$$

which comprise six equations for six variables. They can be separated into a set of four and a set of two, the P-SV and SH systems of elastic wave theory (see, for example, Jeffreys 1976), respectively, by introducing potentials. Write

$$\left.\begin{aligned}
u_j &= \partial_j\phi_u + \epsilon_{jk}\partial_k\psi_u,\\
T_{zj} &= \partial_j\phi_T + \epsilon_{jk}\partial_k\psi_T,
\end{aligned}\right\} \tag{2.15}$$

where $\epsilon_{jk} = -\epsilon_{kj}$ and $\epsilon_{12} = 1$. Since ϵ_{11} and ϵ_{22} are zero the system could be solved by decomposition into Helmholtz equations. We use a procedure, outlined below, which, in a uniform medium, is equivalent to solving the Helmholtz equations, but which

makes the incorporation of the boundary data more straightforward. After taking Fourier transforms one obtains, finally,

$$\left.\begin{aligned} \partial_z \tilde{\psi}_u &= \frac{1}{G}\tilde{\psi}_T, \\ \partial_z \tilde{\psi}_T &= (Gk^2 - m\omega^2)\,\tilde{\psi}_u; \end{aligned}\right\} \tag{2.16}$$

$$\left.\begin{aligned} \partial_z \tilde{u}_z &= \frac{1}{2G}\frac{1-2\nu}{1-\nu}\tilde{T}_{zz} + \frac{\nu}{1-\nu}k^2\tilde{\phi}_u, \\ \partial_z \tilde{\phi}_u &= \frac{1}{G}\tilde{\phi}_T - \tilde{u}_z, \\ \partial_z \tilde{T}_{zz} &= k^2\tilde{\phi}_T - m\omega^2\tilde{u}_z, \\ \partial_z \tilde{\phi}_T &= \frac{\nu}{1-\nu}\tilde{T}_{zz} + \left(\frac{2Gk^2}{1-\nu} - m\omega^2\right)\tilde{\phi}_u. \end{aligned}\right\} \tag{2.17}$$

The pair (2.16) is solved by

$$\begin{bmatrix} \tilde{\psi}_u \\ \tilde{\psi}_T \end{bmatrix} = \begin{bmatrix} \operatorname{ch}(\gamma_s z)\dfrac{1}{G\gamma_s}\operatorname{sh}(\gamma_s z) \\ G\gamma_s \operatorname{sh}(\gamma_s z)\operatorname{ch}(\gamma_s z) \end{bmatrix} \begin{bmatrix} \tilde{\psi}_{u0} \\ \tilde{\psi}_{T0} \end{bmatrix}, \tag{2.18}$$

where $\tilde{\psi}_{u0}$ and $\tilde{\psi}_{T0}$ denote the values of $\tilde{\psi}_u$ and $\tilde{\psi}_T$ on the lower face, $z = 0$, ch and sh denote hyperbolic cosine and hyperbolic sine respectively, and γ_s is an effective wavenumber defined by

$$\gamma_s = \left[k^2 - \frac{m\omega^2}{G}\right]^{\frac{1}{2}}, \quad \operatorname{Re}\gamma_s > 0. \tag{2.19}$$

The system (2.17) is rather more complicated but it can be solved by making a change of variables†

$$\left.\begin{aligned} \tilde{u}_z &= u^s + u^p \\ \tilde{\phi}_u &= \phi^s + \phi^p \\ \tilde{T}_{zz} &= 2Gk^2\phi^s + (2Gk^2 - m\omega^2)\,\phi^p \\ \tilde{\phi}_T &= \frac{1}{k^2}(2Gk^2 - m\omega^2)\,u^s + 2Gu^p \end{aligned}\right\} \tag{2.20}$$

which leads to a separation of the equations. They are solved by

$$\begin{bmatrix} u^s \\ \phi^s \end{bmatrix} = \begin{bmatrix} \operatorname{ch}(\gamma_s z)\dfrac{k^2}{\gamma_s}\operatorname{sh}(\gamma_s z) \\ \dfrac{\gamma_s}{k^2}\operatorname{sh}(\gamma_s z)\operatorname{ch}(\gamma_s z) \end{bmatrix} \begin{bmatrix} u_0^s \\ \phi_0^s \end{bmatrix}, \tag{2.21a}$$

$$\begin{bmatrix} u^p \\ \phi^p \end{bmatrix} = \begin{bmatrix} \operatorname{ch}(\gamma_p z)\gamma_p \operatorname{sh}(\gamma_p z) \\ \dfrac{1}{\gamma_p}\operatorname{sh}(\gamma_p z)\operatorname{ch}(\gamma_p z) \end{bmatrix} \begin{bmatrix} u_0^p \\ \phi_0^p \end{bmatrix}, \tag{2.21b}$$

where γ_s is given by (2.19) and γ_p by

$$\gamma_p = \left[k^2 - \frac{1-2\nu}{2(1-\nu)}\frac{m\omega^2}{G}\right]^{\frac{1}{2}}, \quad \operatorname{Re}\gamma_p > 0. \tag{2.22}$$

† We are indebted to A. J. Haines (private communication) for this observation.

The results (2.21) can be substituted back into (2.20) to give the solution of the equations (2.17) in terms of boundary data on the face $z = 0$. One finds

$$\left.\begin{aligned}\begin{bmatrix}\tilde{u}_z\\ \tilde{\phi}_u\end{bmatrix} &= \boldsymbol{A}\begin{bmatrix}\tilde{u}_{z0}\\ \tilde{\phi}_{u0}\end{bmatrix}+\boldsymbol{B}\begin{bmatrix}\tilde{T}_{zz0}\\ \tilde{\phi}_{T0}\end{bmatrix},\\ \begin{bmatrix}\tilde{T}_{zz}\\ \tilde{\phi}_T\end{bmatrix} &= \boldsymbol{C}\begin{bmatrix}\tilde{u}_{z0}\\ \tilde{\phi}_{u0}\end{bmatrix}+\boldsymbol{D}\begin{bmatrix}\tilde{T}_{zz0}\\ \tilde{\phi}_{T0}\end{bmatrix},\end{aligned}\right\} \tag{2.23}$$

where $\boldsymbol{A}, \ldots \boldsymbol{D}$ are 2×2 matrices, listed in Strathdee *et al.* (1989), with elements which are regular in the neighbourhood of $\omega = 0, k_j = 0$ so that the low-frequency and long-wave limits are well defined.

The solutions (2.18) and (2.23) express the displacements and stresses as functions of boundary data on the interface, $z = 0$. To solve the problem of a load on the upper surface $z = h$ we need the displacement and stress as functions of boundary data on $z = h$. The required expressions can be found by straightforward algebra (details in Strathdee *et al.* 1989) to be

$$\left.\begin{aligned}\tilde{\psi}_u &= \frac{1}{G\gamma_s}\frac{\mathrm{ch}\,(\gamma_s z)}{\mathrm{sh}\,(\gamma_s h)}\tilde{\psi}_{Th}, \qquad \tilde{\psi}_T = \frac{\mathrm{sh}\,(\gamma_s z)}{\mathrm{sh}\,(\gamma_s h)}\tilde{\psi}_{Th},\\ \begin{bmatrix}\tilde{u}_z\\ \tilde{\phi}_u\end{bmatrix} &= (\boldsymbol{A}(z)+\boldsymbol{B}(z)\boldsymbol{E})(\boldsymbol{C}(h)+\boldsymbol{D}(h)\boldsymbol{E})^{-1}\begin{bmatrix}\tilde{T}_{zzh}\\ \tilde{\phi}_{Th}\end{bmatrix},\\ \begin{bmatrix}\tilde{T}_{zz}\\ \tilde{\phi}_T\end{bmatrix} &= (\boldsymbol{C}(z)+\boldsymbol{D}(z)\boldsymbol{E})(\boldsymbol{C}(h)+\boldsymbol{D}(h)\boldsymbol{E})^{-1}\begin{bmatrix}\tilde{T}_{zzh}\\ \tilde{\phi}_{Th}\end{bmatrix},\end{aligned}\right\} \tag{2.24}$$

where, for a non-viscous fluid, $\boldsymbol{E}$ is the 2×2 matrix $\begin{pmatrix}E_{11} & 0\\ 0 & 0\end{pmatrix}$, where

$$E_{11} = \rho g - \frac{\rho\omega^2}{k\,\mathrm{th}\,(kH)}. \tag{2.25}$$

The assumed loading (2.6) on the upper face corresponds to the prescription

$$\tilde{\psi}_{Th} = 0, \qquad \begin{bmatrix}\tilde{T}_{zzh}\\ \tilde{\phi}_{Th}\end{bmatrix} = \begin{bmatrix}\tilde{q}\\ 0\end{bmatrix}. \tag{2.26}$$

On substituting these into (2.24) one finds that the transverse response, ψ_u, vanishes whereas the longitudinal system defines two Green's functions, G_ϕ and G_u, such that

$$\tilde{u}_z = G_u\tilde{q} \quad \text{and} \quad \tilde{\phi}_u = G_\phi\tilde{q}. \tag{2.27}$$

For a general loading the Green's functions would involve more components. If, instead of (2.26) we have $\tilde{T}_{zzh} = \tilde{q}$, $\tilde{\phi}_{Th} = \tilde{r}$ and $\tilde{\psi}_{Th} = \tilde{s}$, where $\tilde{q}$, $\tilde{r}$, and $\tilde{s}$ are specified then the general solution takes the form

$$\tilde{\psi}_u = G_\psi\tilde{s}, \quad \begin{bmatrix}\tilde{u}_z\\ \tilde{\phi}_u\end{bmatrix} = \boldsymbol{G}_2\begin{bmatrix}\tilde{q}\\ \tilde{r}\end{bmatrix},$$

where G_ψ and $\boldsymbol{G}_2$ are given by

$$G_\psi = \frac{1}{G\gamma_s}\frac{\mathrm{ch}\,(\gamma_s z)}{\mathrm{sh}\,(\gamma_s h)}, \quad \boldsymbol{G}_2 = \boldsymbol{N}(z)\boldsymbol{M}^{-1},$$

where $$\boldsymbol{N}(z) = \boldsymbol{A}(z)+\boldsymbol{B}(z)\boldsymbol{E}, \quad \boldsymbol{M} = \boldsymbol{C}(h)+\boldsymbol{D}(h)\boldsymbol{E}. \tag{2.28}$$

The Green's functions G_u and G_ϕ are just the 11- and 21-elements of the matrix $\boldsymbol{G}_2$, but they suffice for the uniaxial loading.

According to (2.24) and (2.27)

$$G_u = \frac{N_{11}(z)M_{22} - N_{12}(z)M_{21}}{M_{11}M_{22} - M_{12}M_{21}}, \quad G_\phi = \frac{N_{21}(z)M_{22} - N_{22}(z)M_{21}}{M_{11}M_{22} - M_{12}M_{21}}. \tag{2.29a, b}$$

The dispersion rule for the coupled system defines the locus of singularities of the Green's functions. It is given implicitly by the equation

$$0 = M_{11}M_{22} - M_{12}M_{21}. \tag{2.30}$$

The Green's functions (2.29) are quite complicated in the general case and so in the following we shall be examining various approximations. To conclude here, we list the general expressions for the components of the strain tensor in the plate

$$\left.\begin{aligned} S_{tj} &= -\int \frac{\mathrm{d}^2k\,\mathrm{d}\omega}{(2\pi)^3} k_t k_j G_\phi \tilde{q}\, \mathrm{e}^{\mathrm{i}(\omega t - k_j x_j)}, \\ S_{zj} &= \tfrac{1}{2}\mathrm{i}\int \frac{\mathrm{d}^2k\,\mathrm{d}\omega}{(2\pi)^3} k_j (G_u + \partial_z G_\phi)\, \tilde{q}\, \mathrm{e}^{\mathrm{i}(\omega t - k_j x_j)}, \\ S_{zz} &= \int \frac{\mathrm{d}^2k\,\mathrm{d}\omega}{(2\pi)^3} \partial_z G_u\, \tilde{q}\, \mathrm{e}^{\mathrm{i}(\omega t - k_j x_j)}. \end{aligned}\right\} \tag{2.31}$$

For future application, we give the right-hand sides of (2.29) for $z = h$ and zero fluid viscosity. To streamline the notation it is useful to introduce scaled variables,

$$K = kh, \quad \Gamma_s = \gamma_s h, \quad \Gamma_p = \gamma_p h, \quad \Omega^2 = \frac{mh^2\omega^2}{2G}, \quad \epsilon = \frac{E_{11}h}{2G}. \tag{2.32}$$

The combinations appearing in (2.29) then reduce to

$$\left.\begin{aligned} &N_{11}M_{22} - N_{12}M_{21} \\ &\quad = \frac{2G}{h}\frac{1}{\Omega^4}\Big[\Omega^2 K^2 \Gamma_p \operatorname{sh}\Gamma_p \operatorname{ch}\Gamma_s - \Omega^2(K^2-\Omega^2)^2 \frac{\operatorname{sh}(\Gamma_s)\operatorname{ch}(\Gamma_p)}{\Gamma_s} \\ &\qquad + \Omega^4 \epsilon \frac{\Gamma_p \operatorname{sh}\Gamma_p \operatorname{sh}\Gamma_s}{\Gamma_s}\Big], \\ &N_{21}M_{22} - N_{22}M_{21} \\ &\quad = \frac{2G}{\Omega^4}\Big[-(K^2-\Omega^2)(2K^2-\Omega^2)(\operatorname{ch}\Gamma_s \operatorname{ch}\Gamma_p - 1) \\ &\qquad + \Big(K^2\Gamma_s\Gamma_p + \frac{(k^2-\Omega^2)^3}{\Gamma_s\Gamma_p}\Big)\operatorname{sh}\Gamma_s \operatorname{sh}\Gamma_p \\ &\qquad + \Omega^2\epsilon\Big(\Gamma_p \operatorname{sh}\Gamma_p \operatorname{ch}\Gamma_s - (K^2-\Omega^2)\frac{\operatorname{sh}\Gamma_s \operatorname{ch}\Gamma_p}{\Gamma_s}\Big)\Big], \\ &M_{11}M_{22} - M_{12}M_{21} \\ &\quad = \Big(\frac{2G}{h}\Big)^2 \frac{1}{\Omega^4}\Big[-2K^2(2K^2-\Omega^2)^2(\operatorname{ch}\Gamma_s \operatorname{ch}\Gamma_p - 1) \\ &\qquad + \Big(K^4\Gamma_s\Gamma_p + \frac{(K^2-\Omega^2)^4}{\Gamma_s\Gamma_p}\Big)\operatorname{sh}\Gamma_s \operatorname{sh}\Gamma_p \\ &\qquad + \Omega^2\epsilon\Big(K^2\Gamma_p \operatorname{sh}\Gamma_p \operatorname{ch}\Gamma_s - (K^2-\Omega^2)^2\frac{\operatorname{sh}\Gamma_s \operatorname{ch}\Gamma_p}{\Gamma_s}\Big)\Big]. \end{aligned}\right\} \tag{2.33}$$

For $\omega^2 \ll Gk^2/m$, that is $U \ll (G/m)^{\frac{1}{2}} \approx 2\times 10^3\ \mathrm{ms}^{-1}$, equations (2.19) and (2.22) can be expanded in powers of ω^2. Consequently, for practical values of the vehicle speed U, (2.33) may be written

$$N_{11}M_{22}-N_{12}M_{21} = \left(\frac{2G}{h}\right)(a_u + b_u\omega^2), \tag{2.34a}$$

where

$$\left.\begin{aligned} a_u &= (1-\zeta)[K^2 + K\,\mathrm{ch}\,K\,\mathrm{sh}\,K + \beta^2\,\mathrm{sh}^2K], \\ b_u &= -\frac{1}{4}\left(\frac{mh^2}{G}\right)\left\{1-\zeta^2+2(1-\zeta^2)\,\mathrm{sh}^2K+(\zeta^2+1)\frac{\mathrm{ch}\,K\,\mathrm{sh}\,K}{K}\right. \\ &\quad \left.+\beta^2\left[2(1-\zeta^2)\frac{\mathrm{ch}\,K\,\mathrm{sh}\,K}{K}-2(1-\zeta)^2\frac{\mathrm{sh}^2K}{K^2}\right]+4r\frac{\mathrm{sh}^2K}{K}\right\}, \\ N_{21}M_{22}-N_{22}M_{21} &= 2G(a_\phi + b_\phi\omega^2), \end{aligned}\right\} \tag{2.34b}$$

where

$$\left.\begin{aligned} a_\phi &= -(\zeta-1)^2K^2+\zeta(\zeta-1)\,\mathrm{sh}^2K+(\zeta-1)^2\beta^2+\zeta(\zeta-1)\beta^2\frac{\mathrm{ch}\,K\,\mathrm{sh}\,K}{K}, \\ b_\phi &= \frac{1}{4}\frac{mh^2}{G}\left\{(-2\zeta^3+5\zeta^2-4\zeta+1)+2(\zeta-\zeta^3)\frac{\mathrm{ch}\,K\,\mathrm{sh}\,K}{K}\right. \\ &\quad +(4\zeta^3-5\zeta^2+4\zeta-1)\frac{\mathrm{sh}^2K}{K^2} \\ &\quad +\beta^2\left[2(\zeta-\zeta^3)\frac{\mathrm{sh}^2K}{K^2}+(\zeta^3-\zeta^2+\zeta-1)\frac{\mathrm{ch}\,K\,\mathrm{sh}\,K}{K^3}+\frac{-\zeta^3+\zeta^2-\zeta+1}{K^2}\right] \\ &\quad \left.+r\left[4\zeta\frac{\mathrm{ch}\,K\,\mathrm{sh}\,K}{K^2}+4(\zeta-1)/K\right]\right\}, \\ M_{11}M_{22}-M_{12}M_{21} &= \left(\frac{2G}{h}\right)^2(a_d+b_d\omega^2), \end{aligned}\right\} \tag{2.43c}$$

where

$$a_d = (1-\zeta)^2[K^2\,\mathrm{sh}^2K - K^4 + \beta^2(K^2 + K\,\mathrm{ch}\,K\,\mathrm{sh}\,K)],$$

$$\begin{aligned} b_d = \frac{1}{4}\frac{mh^2}{G}\Big\{&4(\zeta^3-2\zeta^2+2\zeta-1)\,\mathrm{sh}^2K-2(\zeta^3-\zeta^2-\zeta+1)K\,\mathrm{ch}\,K\,\mathrm{sh}\,K \\ &-2(\zeta^3-3\zeta^2+3\zeta-1)K^2+\beta^2\Big[-2(\zeta^3-\zeta^2-\zeta+1)\,\mathrm{sh}^2K \\ &+(\zeta^3-\zeta^2+\zeta-1)\frac{\mathrm{ch}\,K\,\mathrm{sh}\,K}{K}-(\zeta^3-\zeta^2-\zeta+1)\Big]-4r(1-\zeta)[K+\mathrm{ch}\,K\,\mathrm{sh}\,K]\Big\}; \end{aligned}$$

and

$$\zeta = \frac{1-2\nu}{2(1-\nu)}, \quad \beta^2 = \frac{\rho gh}{2G(1-\zeta)}, \quad r = \frac{\rho}{2m\,\mathrm{th}\,(kH)}.$$

3. Stationary limit

In this section we discuss the zero frequency limit of (2.33). This limit corresponds to a stationary load. In this context we take the 'steady-state' solution to mean the solution that applies at timescales long compared with transients but short compared with creep phenomena, hence we do not consider the effects of creep.

From (2.29) and (2.34) the zero-frequency limits of the Green's functions G_ϕ and G_u on the upper face, $z = h$, are

$$\left.\begin{aligned} G_u &= \frac{h}{2G(1-\zeta)} \frac{1+\frac{\operatorname{sh} K \operatorname{ch} K}{K}+\beta^2\frac{\operatorname{sh}^2 K}{K^2}}{\operatorname{sh}^2 K - K^2 + \beta^2\left(1+\frac{\operatorname{sh} K \operatorname{ch} K}{K}\right)} \\ G_\phi &= \frac{h^2}{2G} \frac{-\left(1+\frac{\zeta}{1-\zeta}\frac{\operatorname{sh}^2 K}{K^2}\right)+\frac{\beta^2}{K^2}\left(1-\frac{\zeta}{1-\zeta}\frac{\operatorname{sh} K \operatorname{ch} K}{K}\right)}{\operatorname{sh}^2 K - K^2 + \beta^2\left(1+\frac{\operatorname{sh} K \operatorname{ch} K}{K}\right)} \end{aligned}\right\} \tag{3.1}$$

Equally simple results could be obtained for the derivatives $\partial_z G_\phi$ and $\partial_z G_u$, evaluated on the upper face, but we shall not pursue this computation. The object of prime importance here is the Green's function G_ϕ, given in (3.1), from which it is possible to compute the in-plane components S_{ij} of the superficial strain, using (2.31).

Now consider the long-range form of the static integrals. They are generally dominated by exponentially decreasing terms associated with poles of the Green's functions in the half-plane, $\operatorname{Im} K > 0$. According to (3.1) such poles are given by solutions of the equation

$$0 = \operatorname{sh}^2 K - K^2 + \beta^2\left(1+\frac{\operatorname{sh} K \operatorname{ch} K}{K}\right) \tag{3.2}$$

and in G_ϕ there is a pole at $K = 0$ which must be taken into account. The equation (3.2) has infinitely many solutions but, for an asymptotic development, one needs those nearest the real axis. The investigation is much simplified by the fact that β^2 is a small parameter in cases of interest ($\sim 10^{-6}$ for Antarctic sea ice) and a solution is obtained by expanding in powers of K,

$$0 = \tfrac{1}{3}K^4 + 2\beta^2 + \ldots. \tag{3.3}$$

Thus, one finds a zero at the point

$$K \approx e^{i\pi/4}|6\beta^2|^{\frac{1}{4}}(1+O(\beta)) \tag{3.4}$$

and another at the conjugate point $-K^*$. The long-range field is therefore dominated by the damped oscillations

$$\begin{aligned} &\sim \operatorname{Re}[e^{iKr/h}] \\ &= \operatorname{Re}[\exp(-1+i)(\tfrac{3}{2}\beta^2)^{\frac{1}{4}} r/h]. \end{aligned}$$

The decay length is given by $(\tfrac{3}{2}\beta^2)^{-\frac{1}{4}} h = \sqrt{2}l$, (3.5)

where l is the characteristic length mentioned in §1.

One may conclude that, because of the small magnitude of β^2, it is adequate for asymptotic purposes to retain only the leading terms in an expansion in powers of K:

$$\left.\begin{aligned} G_u &\approx \frac{h}{2G(1-\zeta)} \frac{1}{\frac{1}{6}K^4+\beta^2}, \\ G_\phi &\approx -\frac{h^2}{4G(1-\zeta)} \frac{1}{\frac{1}{6}K^4+\beta^2} + \frac{h^2}{2G}\frac{1-2\zeta}{2(1-\zeta)}\frac{1}{K^2}. \end{aligned}\right\} \tag{3.6}$$

The pole at $K^2 = 0$ gives rise to a long-range shear strain which is independent of plate thickness as well as fluid density. It takes the form

$$S_{ij}^{\text{long}} = \frac{\nu}{2G}\partial_i\partial_j \int \frac{\mathrm{d}^2k}{(2\pi)^2}\frac{\tilde{q}(0)}{k^2}\mathrm{e}^{\mathrm{i}kx}$$

$$= \frac{\nu\tilde{q}(0)}{4\pi G}\partial_i\partial_j \ln(r). \tag{3.7}$$

Since it falls like r^{-2}, this term must eventually dominate the exponentially decaying contributions. (The exponential term, due to the singularity (3.4), is discussed in §4. See (4.16).) They become comparable when

$$\frac{\nu\tilde{q}}{4\pi G}\frac{1}{r^2} \sim \frac{3}{4}\frac{(1-\nu)\,\tilde{q}}{Gh^2}\frac{1}{(2\pi)^{\frac{1}{2}}}\left(\frac{l}{r}\right)^{\frac{1}{2}}\mathrm{e}^{-r/\sqrt{2}l}$$

or

$$\left(\frac{r}{l}\right)^{\frac{3}{2}}\mathrm{e}^{-r/\sqrt{2}l} \sim \frac{2\nu}{1-\nu}\frac{\beta}{(3\pi)^{\frac{1}{2}}}. \tag{3.8}$$

With β equal to a few thousandths this equation suggests that the power-law term (3.7) will begin to dominate the strain at $r \sim 15l$, but this is beyond the range of practical significance.

At the other extreme, the response at very short distances is dominated by the large wavenumbers. For this limit the smallness of β is irrelevant and the thin-plate approximation cannot be used. For example, the static Green's functions on the upper face (3.1) give

$$u_z \approx \frac{1-\nu}{G}\int \frac{\mathrm{d}^2k}{(2\pi)^2}\tilde{q}(k)\,\mathrm{e}^{\mathrm{i}kx}\left(\frac{1}{k}+\ldots\right)$$

$$= \frac{1-\nu}{2\pi G}\int \mathrm{d}^2x'\frac{q(x')}{|x'-x|}+\ldots, \tag{3.9a}$$

$$\phi_u \approx \frac{1}{2G}\int \frac{\mathrm{d}^2k}{(2\pi)^2}\tilde{q}(k)\,\mathrm{e}^{\mathrm{i}kx}\left(-\frac{\zeta}{1-\zeta}\frac{1}{k^2}+\ldots\right)$$

$$= \frac{1-2\nu}{4\pi G}\int \mathrm{d}^2x' q(x')\ln|x'-x|+\ldots, \tag{3.9b}$$

where the Euclidean distance from x' is indicated,

$$|x'-x| = [(x'-x)^2+(y'-y)^2]^{\frac{1}{2}}. \tag{3.10}$$

In this approximation, the short-distance distributions of displacement on the upper surface are independent of plate thickness. They are qualitatively different from what would be obtained from a naive application of the thin-plate approximation.

The vertical and horizontal displacements are easily found either by using a fast Fourier transform routine to calculate the discretized transforms of (3.1) or by converting to the Hankel transforms

$$G_u(r) = \frac{1}{2\pi}\int_0^\infty G_u(k)\,J_0(kr)\,k\,\mathrm{d}k, \tag{3.11a}$$

$$\frac{\mathrm{d}}{\mathrm{d}r}G_\phi(r) = -\frac{1}{2\pi}\int_0^\infty G_\phi(k)\,J_1(kr)\,k^2\,\mathrm{d}k, \tag{3.11b}$$

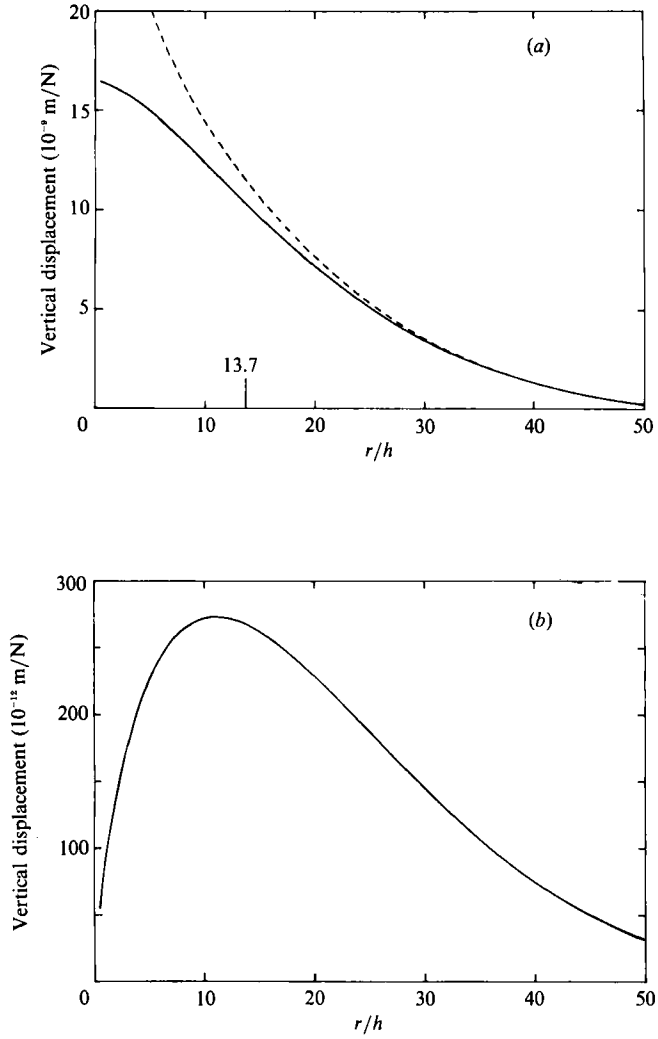

FIGURE 2. (*a*) Vertical displacement versus distance from load computed using (3.11*a*) and (3.1) (solid line) compared with the thin-plate expression (4.16) (dashed line). The vertical line at $r = 13.7h$ marks the characteristic length given by (3.5). (*b*) Horizontal displacement as a function of distance from the load in the static case. The ice sheet thickness $h = 2$ m which corresponds to a value of 0.48×10^{-5} for the coupling parameter β^2 using the parameters shown in the table.

which facilitates the comparison with the large-r expression (4.17), and the small-r expressions (3.9). Figure 2 shows the vertical and horizontal displacements as a function of r. Figures 3 and 2(*a*) compare the vertical displacement computed using (3.11*a*) with the small-r expression (3.9*a*) and the large-r (asymptotic thin plate) expression (4.16). The $1/r$ singularity at the origin is an artefact of the δ-function load; for a load covering a finite area the response would be finite. For $h = 2$ m the asymptotic thin-plate ($r/h \gg 1$) approximation is accurate to within 5% for $r \geqslant 20h$ and to within 10% for $r \geqslant 15h$. So, as could be expected, the asymptotic thin-plate approximation is useful for $r \geqslant l$, where l is the characteristic length given by (1.2). Similar results were found for other values of h in the range 1–100 m and also for the horizontal displacement.

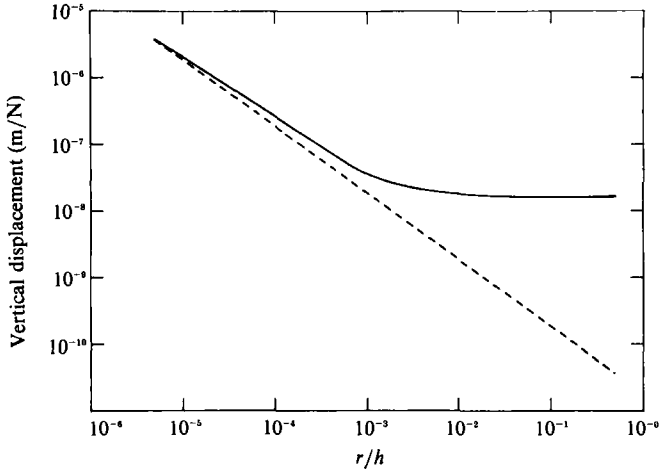

FIGURE 3. The vertical displacement versus distance from load computed using equations (3.11*a*) and (3.1) (solid line) compared with the small-r approximation (3.9*a*) (dashed line). For these calculations $h = 2$ m and $\beta^2 = 0.48 \times 10^{-5}$.

4. Asymptotics and damping

In this section we review the qualitative behaviour of the steady-state pattern as the load speed is varied, including the effects of damping. To do this we use small-k expansions of the expressions giving G_u and G_ϕ corresponding to the thin-plate approximation which we show to be consistent when $\beta^2 \ll 1$. Details of our mathematical development are given in Strathdee *et al.* (1989). For a comprehensive description of steady-state behaviour in the thin-plate approximation, see Davys *et al.* (1985), Schulkes *et al.* (1987) and Hosking *et al.* (1988).

The long-range behaviour of Fourier integrals – such as formula (2.31) for the strain generated by a moving load distribution – is governed by singularities of the integrand. In particular, for the uniformly moving load, the steady-state pattern is dominated at large distances by the contributions of simple poles in the Green's function, G_u and G_ϕ, defined by (2.29). These poles are necessarily among the zeros of the function

$$\det \boldsymbol{M} = \det (\boldsymbol{C}(h) + \boldsymbol{D}(h)\, \boldsymbol{E}) \tag{4.1}$$

where $\boldsymbol{C}(z)$, $\boldsymbol{D}(z)$ and $\boldsymbol{E}$ are the 2×2 matrices mentioned in §2. The determinant (4.1) is a function of k_1, k_2 and ω in general but, for the steady-state pattern, is restricted to the subspace, $\omega = Uk_1$, where U is the load speed.

Owing to the small value of the parameter β^2, defined by (2.34), the asymptotically important zeros of $\det \boldsymbol{M}$ occur at small values of $K = hk$. The thin-plate approximation is therefore appropriate for their determination, exactly as discussed above in the static case.

Another simplification concerns the roles of damping terms. These generally act by causing small imaginary displacements in the zeros of $\det \boldsymbol{M}$. If the zero was originally lying on the real axis, then it would be shifted so as to make the Fourier integral well defined. Once the integration contour has been correctly routed around the singularities, the damping may be turned off. The integral will not be particularly sensitive if the damping is weak. However, this will not be true if it should happen that two zeros of $\det \boldsymbol{M}$ come together in such a way as to pinch the integration contour when the damping is removed. The integral in this case is sensitive to the

small damping and, indeed, would diverge in the limit of vanishing damping. For the problem at hand there is one critical speed, $U = U_c$, at which this happens. It is associated with the threshold for the onset of energy radiation. The pinch is averted by taking into account the damping of the plate.

There is another threshold, $U = U_{c1}$, associated with the extinction of the backward wave, at which two zeros of $\det \boldsymbol{M}$ come together in the absence of damping. In this case, however, the zeros both arrive on the same side of the contour and so do not pinch it. The integral remains well defined when the damping is removed.

Expanding $\det \boldsymbol{M}$ and the numerators of the expressions (2.33) in the small-K limit assuming $\beta^2 \ll 1$ (the thin-plate expansion) one finds

$$G_u \approx \left[D(\omega)\, k^4 + \rho g - \omega^2 \left(mh + \frac{\rho}{k \operatorname{th}(kH)} \right) \right]^{-1}, \tag{4.2a}$$

$$G_\phi \approx -\tfrac{1}{2}h \left(1 - \frac{\beta^2(1-2\zeta)}{h^2 k^2} \right) G_u, \tag{4.2b}$$

where the coefficient D, which may be frequency dependent in (4.3a), is the flexural rigidity, defined by

$$D(\omega) = \tfrac{1}{3}(1-\zeta)\, Gh^3 = \frac{1}{12} \frac{Eh^3}{1-\nu^2}. \tag{4.3}$$

The approximate Green's functions (4.2) are intended to incorporate the singularities whose contributions will dominate the asymptotic behaviour. They can be used only for the asymptotic analysis and not for the general strain and displacement distributions.

Note that G_u vanishes at $k^2 = 0$ if ω^2 is non-vanishing. This means that G_ϕ is regular at $k^2 = 0$ and there will be no long-range contribution at finite frequency. However, if $\omega = Uk_1$ is substituted into (4.2) then, near $k = 0$,

$$\left. \begin{aligned} G_u &\approx \frac{H}{\rho} \frac{k^2}{gHk^2 - U^2 k_1^2}, \\ G_\phi &\approx \frac{\nu}{2G} \frac{gH}{gHk^2 - U^2 k_1^2}. \end{aligned} \right\} \tag{4.4}$$

Although G_u is bounded as $k_j \to 0$, it appears that G_ϕ is singular. This singularity yields a $1/r^2$ term in the asymptotic strain and generalizes the static result (3.6). The static tail in the strain field given by (3.7) is here generalized to

$$\begin{aligned} S_{ij}^{\text{long}} &\approx -\frac{\nu}{2G} \int \frac{\mathrm{d}^2 k}{(2\pi)^2} k_i k_j \tilde{q}(k) \frac{\mathrm{e}^{\mathrm{i}kx}}{(1-v^2)\, k_1^2 + k_2^2} \\ &\approx \frac{\nu}{4\pi G} \frac{\tilde{q}(0)}{(1-v^2)^{\frac{1}{2}}} \partial_i \partial_j \ln \left[\frac{x^2}{1-v^2} + y^2 \right]^{\frac{1}{2}}, \end{aligned} \tag{4.5}$$

where $v^2 = U^2/gH < 1$. This contribution, which follows an inverse square law, will eventually dominate the asymptotic pattern.

Now consider the asymptotic behaviour of the displacement field u_z generated by a load moving with speed U. The singular part of the integrand is approximated by the expression (4.3a) with $\omega = Uk_1$. In a co-moving frame we have

$$u_z = \int \frac{\mathrm{d}^2 k}{(2\pi)^2} \frac{\tilde{q}(k)}{B(k)} \mathrm{e}^{\mathrm{i}kx}, \tag{4.6}$$

where $B(k)$ is given by

$$B(k) = D(Uk_1)\,k^4 + \rho g - U^2 k_1^2 \left(mh + \frac{\rho}{k \operatorname{th}(kH)} \right) \tag{4.7}$$

and $D(Uk_1)$ is given by (4.3) with $\omega = Uk_1$. The asymptotic expansion of (4.6) can be extracted by standard methods (Lighthill 1978). Consideration of the asymptotic expansion shows that $\partial B/\partial \bar{k}_1 = 0$ corresponds to the coalescence of a pair of singularities which happens at the threshold. The rotated integration variable $\bar{k}_1$ is given by

$$\bar{k}_1 = k_1 \cos\theta + k_2 \sin\theta, \quad \bar{k}_2 = -k_1 \sin\theta + k_2 \cos\theta, \tag{4.8}$$

where θ is the angle between the direction of motion and the direction in which the asymptotic field is to be assessed.

This point is characterized by three conditions:

$$\operatorname{Re} B = 0, \quad \frac{\partial \operatorname{Re} B}{\partial k_1} = 0, \quad \frac{\partial \operatorname{Re} B}{\partial k_2} = 0, \tag{4.9}$$

which determine the critical wave vectors $(\pm k_c, 0)$ and the critical speed, U_c. If the small damping term is taken into account then, at $U = U_c$, the solutions will be displaced to complex values of (k_1, k_2) near to the critical points $(\pm k_c, 0)$ and $\partial B/\partial \bar{k}_1$ will be proportional to the damping parameter.

Very approximately, one expects to find

$$\left.\begin{aligned} k_c &\sim \left(\frac{\rho g}{D_0}\right)^{\frac{1}{4}} = \frac{1}{l}, \\ U_c &\sim (gl)^{\frac{1}{2}}, \end{aligned}\right\} \tag{4.10}$$

where l is the characteristic length (Nevel 1970). The consistency of the thin-plate approximation requires

$$hk_c \sim \frac{h}{l} = (6\beta^2)^{\frac{1}{4}} \ll 1.$$

To analyse the wave pattern in the critical region, we can approximate the function B by a quadratic form,

$$B = -a^2 + b(k_1 - k_c - d)^2 + c(k_2)^2 + \ldots, \tag{4.11}$$

where a^2 and d are small quantities, proportional to $(U^2 - U_c^2)$. It is then straightforward to evaluate the asymptotic field,

$$u_z \approx \operatorname{Re}\left[\tilde{q}(k_c, 0)\,(2\pi abc)^{-\frac{1}{2}} \left[\frac{x_1^2}{b} + \frac{x_2^2}{c} \right]^{-\frac{1}{4}} \exp\left(\mathrm{i}a \left[\frac{x_1^2}{b} + \frac{x_2^2}{c} \right]^{\frac{1}{2}} + \mathrm{i}(k_c + d)\,x_1 \right) \right]. \tag{4.12}$$

The parameters $a, \ldots, d$ are obtained from (4.7) by expanding in powers of $k_1 - k_c$, k_2 and $u^2 - u_c^2$.

The effects of damping can be explored by modelling $D(\omega)$ by the Debye relaxation formula together with the assumption that $\omega\tau \sim Uk_c\tau$ is small. We therefore write

$$D(\omega) = \frac{D_0 + \mathrm{i}\omega\tau D_\infty}{1 + \mathrm{i}\omega\tau} \approx D_0 + \mathrm{i}\eta\omega \tag{4.13}$$

where

$$\eta = (D_\infty - D_0)\,\tau.$$

With $\omega\tau$ small and $U \sim U_c$, the parameter a is small and complex,

$$a \sim \left[\left(\frac{U^2}{U_c^2}-1\right)(Dk_c^4+\rho g)+i\eta U k_c^5\right]^{\frac{1}{2}}, \quad \operatorname{Im} a > 0,$$

while bd^2 is negligible in comparison with a^2, and b, c are finite and essentially real. The amplitude (4.12) contains the factor

$$|a|^{-\frac{1}{2}} \sim \left[\left(\frac{U^2}{U_c^2}-1\right)^2 (Dk_c^4+\rho g)^2+\eta^2 U^2 k_c^{10}\right]^{-\frac{1}{8}}$$

and will exhibit a resonant-type peak as U passes through the critical value. The peak amplitude is proportional to $\eta^{-\frac{1}{4}}$ and decreases exponentially with distance from the load, the damping length being of order

$$\frac{|bc|^{\frac{1}{4}}}{|a|} \sim \frac{1}{k_c}(\tau U_c k_c)^{-\frac{1}{2}}. \tag{4.14}$$

In this formula, τ is a relaxation time representing the dissipation in the plate and $1/U_c k_c \sim (l/g)^{\frac{1}{2}}$ is a characteristic time for the threshold motion.

Next consider the other threshold, $U = U_{c1} = (gH)^{\frac{1}{2}}$, at which the backward wave is extinguished. For $U \leqslant U_{c1}$ the zero of $\operatorname{Re} B$ is near the origin and we can use a Taylor expansion about the origin.

For the strictly backward wave only, the asymptotic wave is given by

$$u_z \approx \operatorname{Re}\left[\frac{\tilde{q}(0)}{U^2}\left(\frac{H}{2\pi r}\right)^{\frac{1}{2}}\left(\frac{g}{\rho U^2}\frac{1-U^2/gH}{(mh+\frac{1}{3}\rho H)^3}\right)^{\frac{1}{4}}\exp\left(\tfrac{1}{4}i\pi+ir\left[\frac{\rho g}{U^2}\frac{(1-U^2/gH)}{(mh+\frac{1}{3}\rho H)}\right]^{\frac{1}{2}}\right)\right]. \tag{4.15}$$

This amplitude vanishes at the critical speed.

This concludes the qualitative discussion of the radiative phenomena generated by a moving load. For speeds below threshold, $U < U_c$, there is no radiation. This means that $\operatorname{Re} B$ has no real zeros. In order to apply the asymptotic formula it is necessary to search for zeros in the half-plane $\operatorname{Im} \bar{k}_1 > 0$. For example, in the static limit, with

$$B = D_0 k^4 + \rho g,$$

the asymptotic displacement formula for the static case is given by

$$u_z^{\text{static}} \approx \operatorname{Re}\left[\tilde{q}\frac{1}{(2\pi r)^{\frac{1}{2}}}\frac{l^{\frac{5}{2}}}{2D_0}\exp\left\{-\frac{r}{\sqrt{2l}}+i\left(\frac{r}{\sqrt{2l}}-\frac{3}{8}\pi\right)\right\}\right]. \tag{4.16}$$

The asymptotic pattern is therefore an exponentially damped wave of length $\sqrt{2l}$. For non-vanishing load speeds the exponential damping will persist albeit with angular variation and a lengthening of the damping scale from $\sqrt{2l}$ at $U = 0$ to something like the scale indicated in (4.14) at $U = U_c$.

5. Examples

To demonstrate the way in which the ice displacement depends on the speed of the load we calculated the vertical displacement as a function of distance along the line on which the load was moving (the x-axis) for various speeds. We considered speeds from 0 ms^{-1} to 45 ms^{-1} covering the range both above and below the critical speed, which was found to be approximately 21 ms^{-1} by numerical solution of (4.9) using the parameters shown in table 1. For these speeds the small-ω expressions (2.34) must be used for numerical work because large cancellations in (2.33) make them numerically unstable.

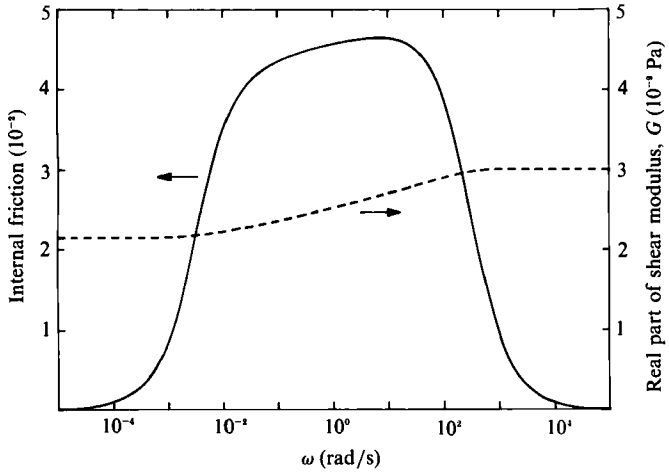

FIGURE 4. The real part of the shear modulus (dashed line, right-hand scale) and the coefficient of internal friction (solid line, left-hand scale) as a function of frequency in the assumed model of the damping.

The vertical displacement for a point load is given by

$$G_u(x) = \frac{1}{(2\pi)^2}\int_{-\infty}^{\infty}\int_{-\infty}^{\infty} G_u(k_x, k_y)\,\mathrm{e}^{-\mathrm{i}(k_x x + k_y y)}\,\mathrm{d}k_x\,\mathrm{d}k_y, \tag{5.1}$$

where $G_u(k_x, k_y)$ is given by (2.34*a*) and (2.34*c*) with $\omega = Uk_x$. For distributed loads the displacement can be found by convoluting (5.1) with the load distribution $q(x, y)$ (see (2.11)). The main effect of this will be to smooth out structures in the displacement versus distance curve with lengthscales less than the lengthscale of the load distribution. For load speeds below the critical speed the displacement is easily calculated by discretizing (5.1) and using a fast Fourier transform routine. For load speeds above the critical speed the denominator (2.34*c*) has real zeros which make the calculation of (5.1) unstable. To overcome this problem we use the fact that, if the contour $\mathrm{Im}\,(k_x) = \lambda$ completed at infinity encloses the same poles as the contour $\mathrm{Im}\,(k_x) = 0$ completed at infinity, then by Cauchy's theorem

$$\int_{-\infty}^{\infty}\int_{-\infty}^{\infty} G_u(k_x + \mathrm{i}\lambda, k_y)\,\mathrm{e}^{-\mathrm{i}(k_x(x+\mathrm{i}\lambda)+k_y y)}\,\mathrm{d}k_x\,\mathrm{d}k_y = \int_{-\infty}^{\infty}\int_{-\infty}^{\infty} G_u(k_x, k_y(\,\mathrm{e}^{-\mathrm{i}(k_x x + k_y y)}\,\mathrm{d}k_x\,\mathrm{d}k_y,$$

so

$$G_u(x) = \frac{1}{(2\pi)^2}\int_{-\infty}^{\infty} \mathrm{e}^{+\lambda x}\left[\int_{-\infty}^{\infty} G_u(k_x + \mathrm{i}\lambda, k_y)\,\mathrm{e}^{-\mathrm{i}k_x x}\,\mathrm{d}k_x\right]\mathrm{d}k_y \tag{5.2}$$

for $y = 0$. (Depending on the behaviour of the poles of $G_u(k_x, k_y)$ it may be necessary for λ to vary with k_y.)

Physical damping must be included in the calculations so that the integrals do not diverge near the critical speed. This is accomplished by taking the shear modulus (and at least one of the bulk modulus and Poisson's ratio) to be complex and frequency dependent. Since the dominant frequency of the radiated waves depends on load speed, we used an approximately constant damping over the range $\omega = 10^{-2}\ \mathrm{s}^{-2}$ to $\omega = 10^{2}\ \mathrm{s}^{-2}$ given by

$$\frac{1}{G} = \frac{1}{G_\infty}\left[1 + \frac{1}{\pi Q}\log_{\mathrm{e}}\left(\frac{\omega - \mathrm{i}\omega_\infty}{\omega - \mathrm{i}\omega_0}\right)\right]^2, \tag{5.3}$$

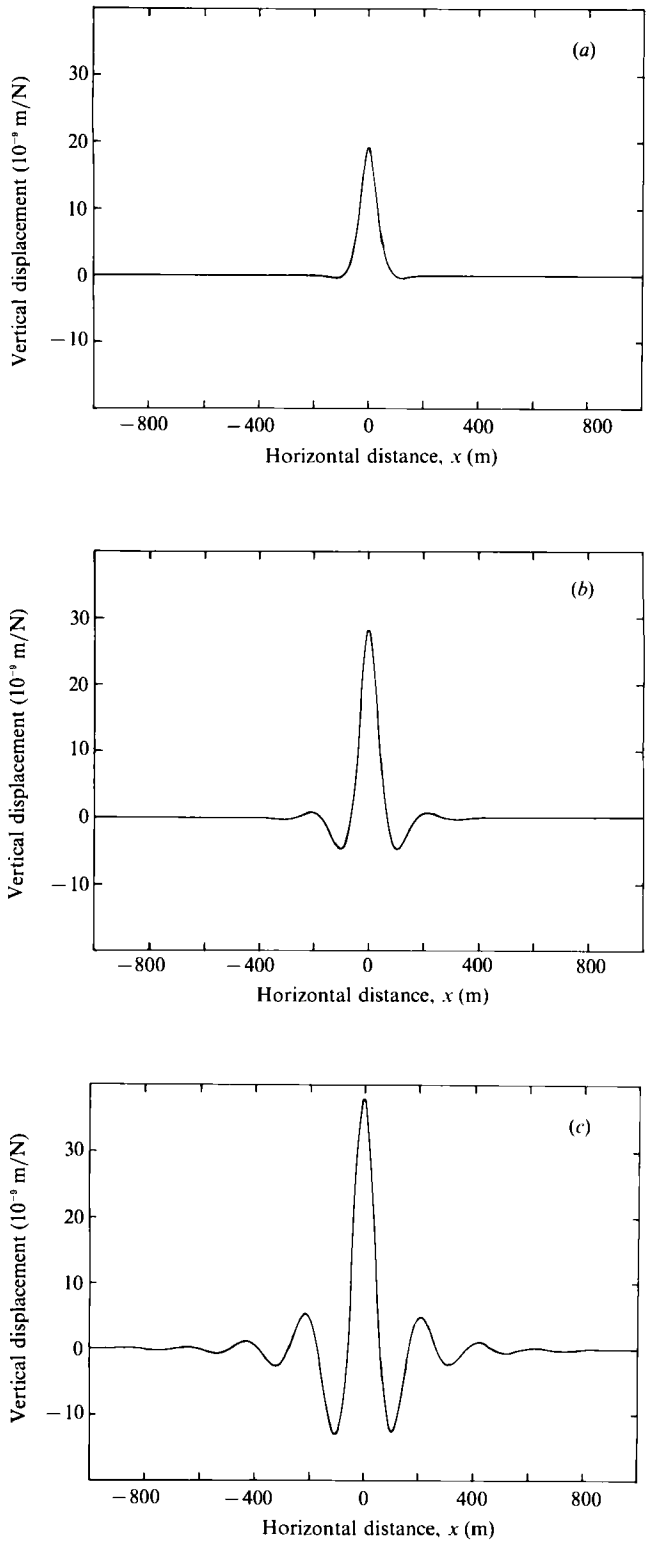

FIGURE 5(*a–c*). For caption see facing page.

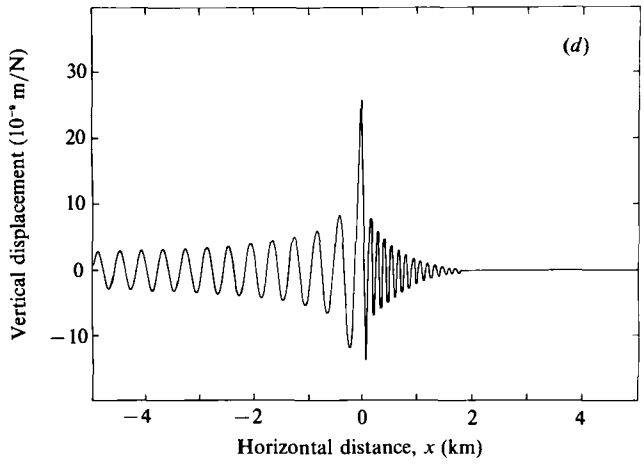

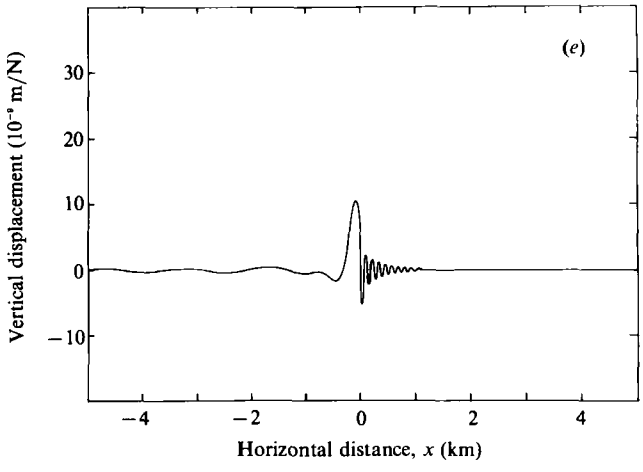

FIGURE 5. Vertical displacement as a function of distance along the x-axis for a load moving along the x-axis with velocity (*a*) 0 ms^{-1}, (*b*) 17.5 ms^{-1}, (*c*) 20 ms^{-1}, (*d*) 25 ms^{-1}, (*e*) 45 ms^{-1}. Other parameters are as shown in table 1.

where ω_0 and ω_0 determine the range over which damping is significant. This form of $G(\omega)$ can be derived from a superposition of exponential memory functions with constant strength for which the relaxation time is continuously distributed (see the Appendix). Models of this type have been found to apply to other complex geophysical media (Aki & Richards 1980). The value of Q was chosen to be 20 so that the decay of the calculated forward-radiating flexural wave was similar to that observed by Squire *et al.* (1988) (the backward-radiating gravity wave is not strongly affected by attenuation in the ice sheet). The frequency dependence of the real part of the shear modulus and the coefficient of internal friction, Q^{-1}, in this model are shown in figure 4. A more appropriate model for the damping can easily be incorporated when more data on attenuation in sea ice become available.

The results for the vertical displacement as a function of distance along the x-axis for a moving load are shown in figure 5. They show the same features identified previously both experimentally (e.g. Squire *et al.* 1988; Takizawa 1988), and

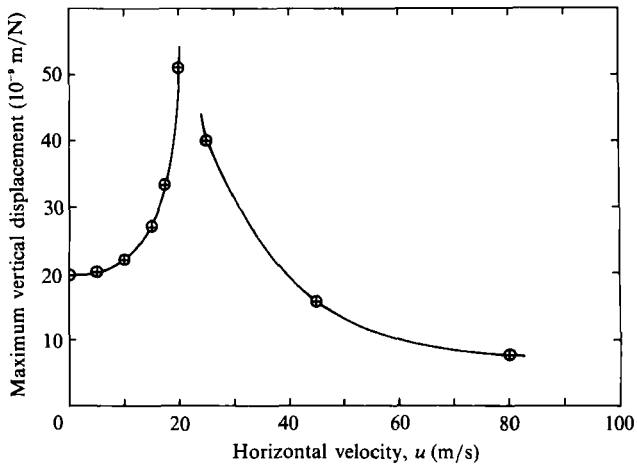

FIGURE 6. Maximum vertical displacement as a function of load speed.

theoretically (e.g. Hosking *et al.* 1988; Davys *et al.* 1985), namely a quasi-static region ($u < 17.5$ ms^{-1}), a transition region (17.5 ms^{-1} $< u <$ 21 ms^{-1}), a region with backward- and forward-radiating waves (21 ms^{-1} $< u <$ 55 ms^{-1}), and the gradual extinction of the backward wave as u approaches $(gH)^{\frac{1}{2}} = 55$ ms^{-1} as expected from the discussion in §4.

The maximum displacement is plotted against load speed in figure 6, which demonstrates how the displacement is amplified by a factor >2.5 near the critical speed in agreement with the above-mentioned experimental results.

In §3 we investigated the validity of asymptotic thin-plate theory for a stationary load and found it to be useful for $r > l$. We would expect a similar result for the validity of asymptotic theory to apply for moving loads since for practical load speeds ($U \ll (G/m)^{\frac{1}{2}}$) the structure of the thick-plate Green's function is the same as that of the thin-plate Green's function; that is, they have essentially the same poles with the same weights.

6. Conclusions

We have developed formulae appropriate to a uniform plate of finite thickness, with a view to describing the near-field response to a concentrated load incorporating the effects of viscous damping in the ice sheet so as to obtain the behaviour at near critical speeds.

The response is given by a pair of Green's functions, G_u and G_ϕ, whose general form is described in §2. Explicit formulae for the values taken by these functions on the upper surface of the plate are contained in (2.33) and (2.34). Equations (2.34) can be used to compute the displacement field at the surface of the ice for any reasonable value of the load speed. Equally explicit formulae for points in the interior could be derived. Such formulae are needed to represent the stress and strain distributions in the near field, i.e. in the vicinity of a concentrated load – one whose spread is comparable with or smaller than the thickness of the plate. The zero-frequency limits of G_u and G_ϕ, given by (3.1), manifest short-wavelength behaviour which is sharply different from that of the classical thin-plate formulae. The corresponding short-distance behaviour of the displacement variables, u_z and ϕ_u, is given by (3.9).

The treatment of the finite-thickness problem given here has, in our view, clarified the limitations of the classical thin-plate theory. The latter is justified by the small value of the coupling parameter β^2 or, equivalently, the condition

$$h \ll \frac{1}{\rho g}\frac{G}{1-\nu}.$$

Corrections to the classical theory, in the form of higher powers of k^2 and ω^2, can be obtained from the formulae derived here. They become increasingly significant as distance from the source is reduced. In fact our calculations indicate that thin-plate theory is in error by greater than 5% for r less than $20h$,

A perhaps surprising result of the general analysis of §2 is the emergence of a long-range component of shear strain. This contribution, which falls off with the square of the distance, must eventually dominate the asymptotic field. But, as shown in §3, for the values of β^2 likely to obtain in practice, the tail would become dominant only at distances on the order of fifteen characteristic lengths.

Finally, the response to a moving load with near critical velocity is sensitive to damping forces, as expected. The asymptotic pattern is given by (4.12) in terms of the critical velocity, U_c, and wavenumber k_c. The amplitude is seen to exhibit a resonant-type peak as the velocity, U, passes through its critical value. We have shown that the peak value is limited by a factor of order

$$\left[\frac{1}{\tau}\left(\frac{l}{g}\right)^{\frac{1}{2}}\right]^{\frac{1}{4}}$$

where τ is a relaxation time characterizing the dissipation in the ice plate, and l is the characteristic length.

For the future, it would be interesting to take into account the effects of residual stresses as well as a layered plate structure. The stresses at various depths near the load can be computed. It will be important to allow for creep of the ice, and also to consider the case of an elastic-plastic plate.

We are very grateful to John Haines for informing us of the seismic techniques and their suitability for the problem of the ice sheet of finite thickness and for advice on computational techniques.

Appendix. The viscoelastic model

Equation (5.3) may be derived by assuming a memory function of the form

$$\epsilon(t) = \frac{1}{G_\infty}\left[\sigma(t) + \int_0^\infty \sigma(t-\tau)\,\Psi(\tau)\,\mathrm{d}\tau\right] \tag{A 1}$$

where ϵ is the strain, σ is the stress, and

$$\Psi(t) = \sum_j A_j\,\mathrm{e}^{-\alpha_j t}, \quad A_j \geqslant 0, \alpha_j \geqslant 0.$$

This is equivalent to

$$\sigma(t) = G_\infty\left[\epsilon(t) - \int_0^\infty \epsilon(t-\tau)\,\Psi(\tau)\,\mathrm{d}\tau\right]$$

with

$$\Psi(t) = \sum_j B_j\,\mathrm{e}^{\beta_j t}, \quad B_j \geqslant 0, \quad \beta_j \geqslant 0$$

(cf. Hosking *et al.* 1988) when the A_j, α_j are related to the B_j, β_j by an appropriate transformation. Taking

$$f(\omega) = \int_{-\infty}^{\infty} f(t)\, e^{i\omega t}\, dt$$

(A 1) implies

$$\frac{1}{G(\omega)} = \frac{1}{G_\infty}\left(1 + \sum_j \frac{A_j}{\alpha_{j-i\omega}}\right), \tag{A 2}$$

so $G(\omega)$ is positive for all frequencies, whatever the values of A_j and α_j. If the relaxation times are continuously distributed then

$$\sum_j \frac{A_j}{\alpha_j - i\omega} = \int_0^\infty \frac{A(\alpha)\, d\alpha}{\alpha - i\omega}$$

and if

$$A(\alpha) = \begin{cases} \eta, & \omega_0 \leqslant \omega \leqslant \omega_\alpha \\ 0, & \text{otherwise,} \end{cases}$$

$$\int_0^\infty \frac{A(\alpha)\, d\alpha}{\alpha - i\omega} = \eta \int_{\omega_0}^{\omega_\infty} \frac{d\alpha}{\alpha - i\omega} = \eta \ln\left(\frac{\omega_\infty - i\omega}{\omega_0 - i\omega}\right).$$

For $\omega_0 \ll \omega \ll \omega_\infty$

$$\ln\left(\frac{\omega_\infty - i\omega}{\omega_0 - i\omega}\right) = \ln\left(\frac{\omega_\infty}{\omega}\right) + \tfrac{1}{2}i\pi$$

so

$$Q = \frac{\operatorname{Re} G(\omega)}{\operatorname{Im} G(\omega)} = \left(\frac{2}{\pi}\right)\left[\frac{1}{\eta} + \ln\left(\frac{\omega_\infty}{\omega}\right)\right],$$

where Q^{-1} is the coefficient of internal friction. If $(1/\eta) \gg \ln(\omega_\infty/\omega)$ then $\eta = 2/(\pi Q)$ and

$$\frac{1}{G(\omega)} = \frac{1}{G_\infty}\left[1 + \frac{2}{\pi Q} \ln\left(\frac{\omega_\infty - i\omega}{\omega_0 - i\omega}\right)\right]. \tag{A 3}$$

Hence, for large Q,

$$\frac{G(\omega_1)}{G(\omega_2)} = 1 + \frac{2}{\pi Q} \ln\left(\frac{\omega_1}{\omega_2}\right) \tag{A 4}$$

and

$$\frac{c(\omega_1)}{c(\omega_2)} = 1 + \frac{1}{\pi Q} \ln\left(\frac{\omega_1}{\omega_2}\right), \tag{A 5}$$

where c is the phase velocity of shear waves given by $(G/m)^{\frac{1}{2}}$.

The square appears in (5.3) because (A 5) was originally discovered empirically for geophysical media (Aki & Richards 1980) and the frequency-dependent shear modulus was taken to be related to the square of the frequency-dependent phase velocity. For large Q (small attenuation) (5.3) and (A 3) are the same.

REFERENCES

Aki, K. & Richards, P. G. 1980 *Quantitative Seismology*, vol. 1, pp. 167–182. San Francisco: W. H. Freeman and Co.

Bates, H. F. & Shapiro, L. H. 1981 Stress amplification under a moving load on floating ice. *J. Geophys. Res.* **86**, 6638.

Beltaos, S. 1981 Field studies on the response of floating ice sheets to moving loads. *Can. J. Civil Engng* **8**, 1.

Davys, J. W., Hosking, R. J. & Sneyd, A. D. 1985 Waves due to a steadily moving source on a floating ice plate. *J. Fluid Mech.* **158**, 269.

DORONIN, YU. P. & KHEISIN, D. E. 1977 *Sea Ice*, p. 156 (English transl.). Office of Polar Programmes and the National Science Foundation, Amerind, New Delhi.

EYRE, D. 1977 The flexural motions of a floating ice sheet induced by moving vehicles. *J. Glaciol.* **19**, 555.

HOSKING, R. J., SNEYD, A. O. & WAUGH, O. W. 1988 Viscoelastic response of a floating ice plate to a steadily moving load. *J. Fluid Mech.* **196**, 409.

JEFFREYS, H. 1976 *The Earth*, p. 28. Cambridge University Press.

KENNETT, B. L. N. 1983 *Seismic Wave Propagation in Stratified Media.* Cambridge University Press.

KERR, A. D. 1976 The bearing capacity of floating ice plate subjected to static or quasistatic loads. *J. Glaciol.* **17**, 229.

KERR, A. D. 1983 The critical velocities of a load moving on a floating ice plate that is subjected to inplane forces. *Cold Regions Sci. Tech.* **6**, 267.

LIGHTHILL, M. J. 1978 *Waves in Fluids.* Cambridge University Press.

NEVEL, D. E. 1970 Moving loads on a floating ice sheet. *US Army CRREL Res. Rep.* 261.

SCHULKES, R. M. S. M., HOSKING, R. J. & SNEYD, A. D. 1987 Waves due to a steadily moving source on a floating ice plate. Part 2. *J. Fluid Mech.* **180**, 297.

SCHULKES, R. M. S. M. & SNEYD, A. D. 1988 Time-dependent response of a floating ice-sheet to a steadily moving load. *J. Fluid Mech.* **186**, 25.

SQUIRE, V. A. & ALLEN, A. J. 1980 Propagation of flexural gravity waves in sea ice. In *Sea Ice Processes and Models* (ed. R. S. Pritchard), p. 237. University of Washington Press.

SQUIRE, V. A., ROBINSON, W. H., HASKELL, T. G. & MOORE, S. C. 1985 Dynamic strain response of lake and sea ice to moving loads. *Cold Regions Sci. Tech.* **11**, 123.

SQUIRE, V. A., ROBINSON, W. H., LANGHORNE, P. J. & HASKELL, T. G. 1988 Vehicles and aircraft on floating ice. *Nature* **333**, 159.

STRATHDEE, J., ROBINSON, W. H. & HAINES, E. M. 1989 Moving loads on ice plates of finite thickness. *DSIR Physics and Engineering Laboratory Report.*

TAKIZAWA, T. 1985 Deflection of a floating sea ice sheet induced by a moving load. *Cold Regions Sci. Tech.* **11**, 171.

TAKIZAWA, T. 1988 Response of a floating sea ice sheet to a steadily moving load. *J. Geophys. Res.* **93**, 5100.